# Investigation of Underbead Hardness In Carbon and Low Alloy Steels

## There is excellent correlation between underbead hardness derived from CTS or RPI Gleeble tests and that calculated from mathematical formulas valid for all low alloy steels

BY J. BRISSON, P. H. MAYNIER, J. DOLLET AND P. BASTIEN

### Introduction

The purpose of the present investigation is to develop a technique for the determination of underbead hardness in low alloy steels, independent of the base metal composition and of single-pass arc welding conditions. The study is a continuation of work already reported elsewhere.[1]

Certain points brought up in the latter study have been investigated in more detail and others are recapitulated. This has enabled us to conclude without restriction that it is possible to determine and therefore to predict the underbead hardness of low alloy steels, whatever the single-pass arc welding conditions.

Although the welding tests which are to be discussed are CTS tests, and therefore cracking tests, it is not explicitly intended to describe here our ideas on underbead cracking. However, this aspect is not completely neglected since we are convinced that a proper understanding of the structure is essential to be able to control underbead hardness. In our opinion, the influence of hydrogen and of stresses cannot properly be grasped without first having determined whether the structure is depending on the steel and the welding conditions—martensitic, bainitic or ferritic.

The authors are associated with the Research Department of Creusot-Loire, Le Creusot, France.

In the first part of this paper it will be shown that to establish the underbead hardness, it is necessary to determine the cooling rate at the weld joint, CTS or otherwise, whatever the welding conditions.

In the second part the CTS test is considered. Each underbead hardness measurement is interpreted with the help of synthetic cycles carried out on the RPI Gleeble machine and compared with mathematical relations between critical cooling rates and hardness.

In this way it is possible, as will be described in the third part, to obtain overall predictions of the underbead hardness at a welded joint or in synthetic tests on the RPI Gleeble machine, whatever the steels and the welding conditions.

### Cooling Rate—Part I

In this first section we shall consider the cooling rate effectively obtained in the welds under investigation, and in particular those resulting from a CTS test. This is a direct consequence of our fundamental principle involving the structure after quenching.

The rate of cooling obtained at a weld depends on a number of physical parameters such as the thermal conductivity of the metal, plate thickness, welding energy and contingent preheating. This cooling rate contrasts with the critical cooling rates during quenching, since the latter depend only on metallurgical factors such as hardenability of the steel.

All correlations of hardness and transformation temperatures have the cooling rate as abscissa. The time taken to cool between, for example, 800 and 500C is sometimes used by other authors but we prefer to employ the cooling rate as a coordinate, since this is the real value of interest. The reference temperature has then only a secondary importance. In the present case we have chosen, like Cottrell, 300C. The reason for employing the logarithm of the cooling rate is, as will be seen below, to enable the use of a simple expression for hardenability.

Two mathematical relations were available to calculate the rate of cooling in CTS tests, that of Cottrell and that of Adams, with which we were particularly familiar.

Since a thorough comparison of these methods is necessary, it is useful to recapitulate briefly the two treatments:

#### Cottrell's Formula

$$V_r \text{ at } 300C = \frac{1}{\left(\frac{122\,Q}{10^6\,N} + 0.05\right)^2}$$

where

N = TSN value

Q = total energy (J/cm)

$V_r$ is in °C/sec

N can readily be related to the plate

thickness. In our CTS tests the thickness of the top plate was always identical to that of the bottom plate. With the thickness e in mm, one then has:

For a bi-thermal bead $N = \frac{8e}{25.4}$ and

For a tri-thermal bead $N' = \frac{12e}{25.4}$

25.4 being the conversion factor from inches to mm.

We emphasize that, while Cottrell proceeded from Rosenthal's basic formula, his equation was also based on experiment, the measurement of cooling rates being comparatively easy. Q thus corresponds to the energy consumed in the arc and not the energy effectively introduced into the weld.

### Adam's Formula

Starting from Rosenthal's basic equation, Adams[9] was able to show that for two-dimensional heat flow, that is with "thin" plates, one has:

$$V_r = 2\pi \cdot \lambda \cdot \rho \cdot C \left(\frac{(e)^2}{(Q)}\right)(T - T_o)^3$$

Equation 1

where:

$V_r$ = cooling rate in °C per sec from temperature T

$\lambda$ = coefficient of thermal conductivity

$\rho C$ = specific heat capacity

e = plate thickness

Q = energy per unit length introduced into the plate by the arc

$T_o$ = initial temperature.

For the steels under investigation, the average values taken for the physical constants were respectively

$\lambda$ = 0.12 cal/cm °C sec

$\rho C$ = 1 cal/cm³ (°C)

In three dimensional heat flow, i.e. in the case of a single-pass deposition on heavy gauge plate ($e \geqslant 50$ mm):

$$V_r = \frac{2\pi\lambda}{Q}(T - T_o)^2$$

Equation 2

For cases which fall between two and three dimensional heat flow, Adams proposed the use of the intermediate factor:

$$E = \rho C e^2 (T - T_o)\frac{1}{Q}$$

Equation 3

in order to determine whether two or three dimensional heat flow is involved. If E does not exceed 0.33, the flow is two dimensional and equation (1)

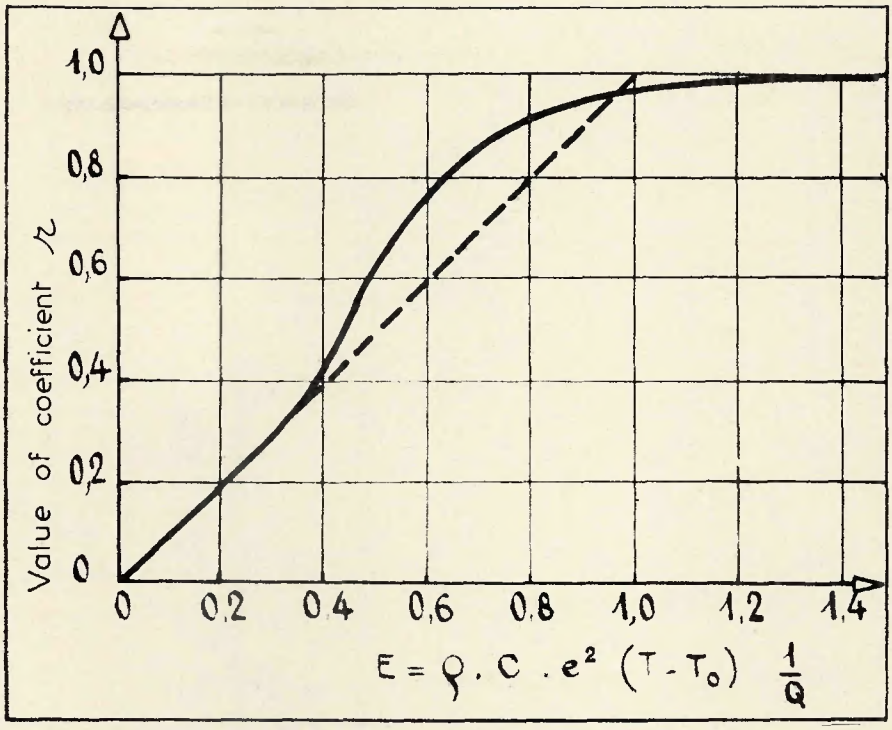


Fig. 1—Graphical solution for determining $V_r$

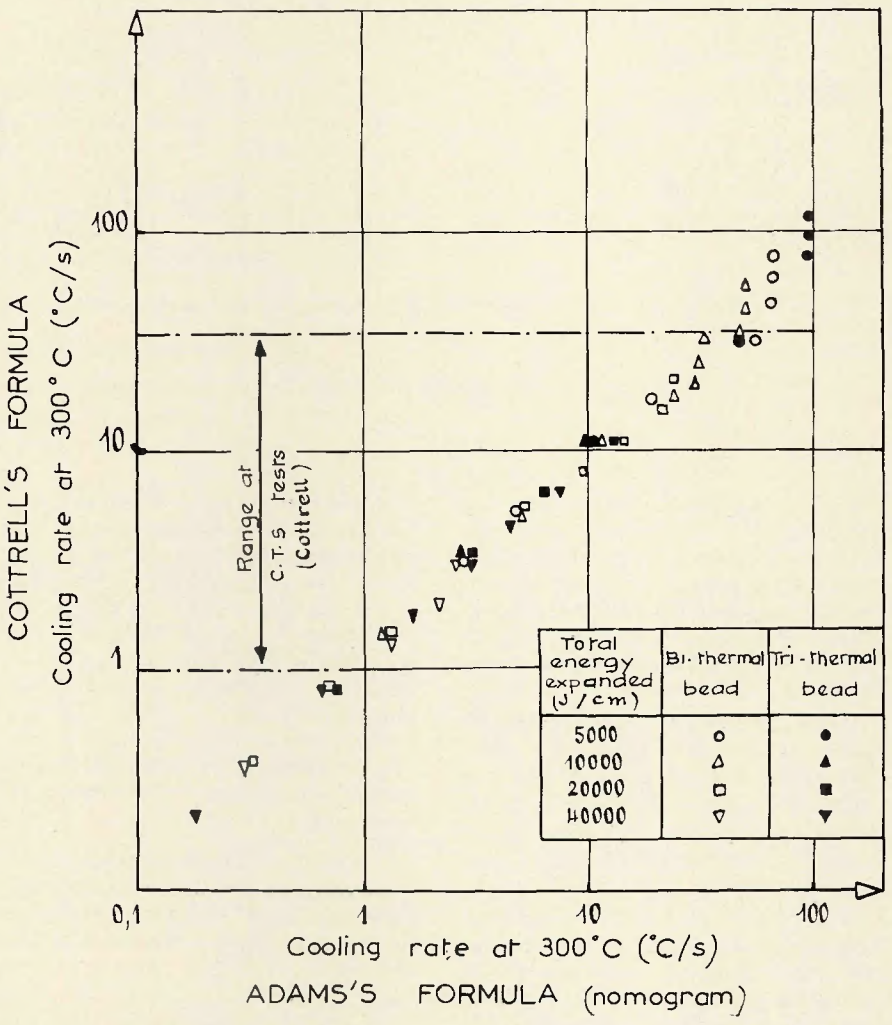


Fig. 2—Comparison of the results of calculating cooling rates by Cottrell's formula and by Adam's formula

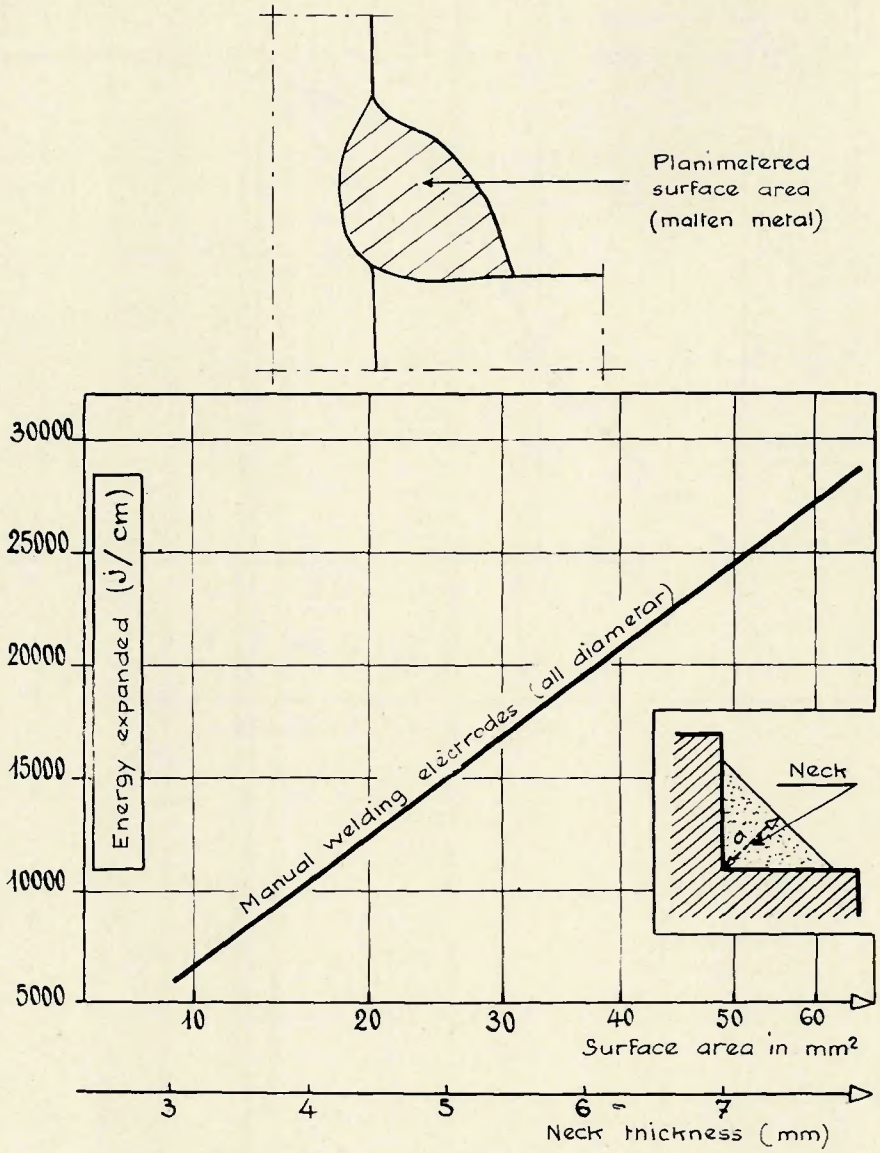


Fig. 3—Cross sectional area of molten metal determined by planimetry

should be used. If E is greater than 1.2, the heat flow is three dimensional and equation (2) should be employed. Between these two values no explicit equation can be established. In this case Adams proposes a graphical solution (Fig. 1) which allows $V_r$ to be determined as a function of r.

In any case, one of the most important merits of Adams's technique is that nomograms can be established, the use of which is extremely convenient; in particular they assist in precluding numerous possible errors due to the units employed.

It has been pointed out earlier that both formulas are derived from Rosenthal's basic equation, but that Cottrell, basing his calculation on experimental results, used the energy consumed and not the energy actually supplied. Thus, by comparing both equations, that is by calculating individual cooling rates, it is possible to derive a value for the efficiency. The results are plotted in Fig. 2. They are equally valid for a bithermal as well as a tri-thermal weld bead. It can be seen that, in CTS tests, the rates of cooling at 300C obtained by the two methods are in good agreement only for an efficiency of $\mu = 75\%$. In our opinion, this is an important result, since the amount of energy effectively used during welding is determined by the efficiency.

In fact it is extremely difficult, even impossible, to evaluate directly the amount of energy effectively introduced into the plates during deposition of the weld bead.

We have

$$Q = \mu \frac{UI}{V}$$

where $\mu$ = efficiency

U = voltage (volts)

I = current (amp)

V = rate of advance (cm/sec).

Whereas U, I and V can usually be measured with moderate accuracy, $\mu$, in contrast is not directly measurable. For this reason we felt it necessary to determine the energy introduced by an indirect method, as pointed out by Cottrell. This consists in measuring the cross sectional area of the molten metal by planimetry (Fig. 3).

This relationship between energy and area of molten metal would be valid for all grades of steel and for all electrode diameters for manual welding (as in a CTS test). However, as stated earlier, it must be emphasized that the energy reported is the energy consumed and not that supplied.

In summary, for a bi-thermal weld bead (CTS) the cooling rate at 300C can be derived using Adams's nomogram, taking care to introduce an efficiency of 75% ($\mu = 0.75$).

For a tri-thermal weld bead (CTS), the cooling rate at 300C is determined from the same nomogram, taking as before, Q = f (S) with an efficiency of 75%, but correcting the energy by a factor of ⅔ (3 directions of heat dissipation).

Finally, it should be noted that clearly known welding conditions can always be plotted on simple charts. In Fig. 4 is shown the relationship for a weld carried out without preheating between cooling rate, energy supplied and plate thickness. For example, for a thickness of 20 mm and an energy of 20 KJ/cm, one obtains $V_r = 3°C/S$ at 300C.

For a preheat of 150C in the same conditions, the cooling rate falls to 0.4°C/S, as shown in Fig. 5.

## The CTS Test—Part II

We shall now consider the CTS test by interpreting each underbead hardness value with the help of simulation tests performed in an RPI "Gleeble" machine using our formulas relating critical cooling rates and hardness.

The tests were conducted essentially on five grades of steel (Table 1). The first two grades are of the A52 type, used after normalizing to a ferrite/pearlite structure. The third grade is a dispersed phase vanadium steel whose yield strength can be as high as 45 to 50 kg/mm² after normalizing and if required, tempering. The last two grades were in the martensitic hardened and tempered condition, the yield strength being greater than 70 kg/mm².

The series of materials investigated thus encompassed an extensive range of

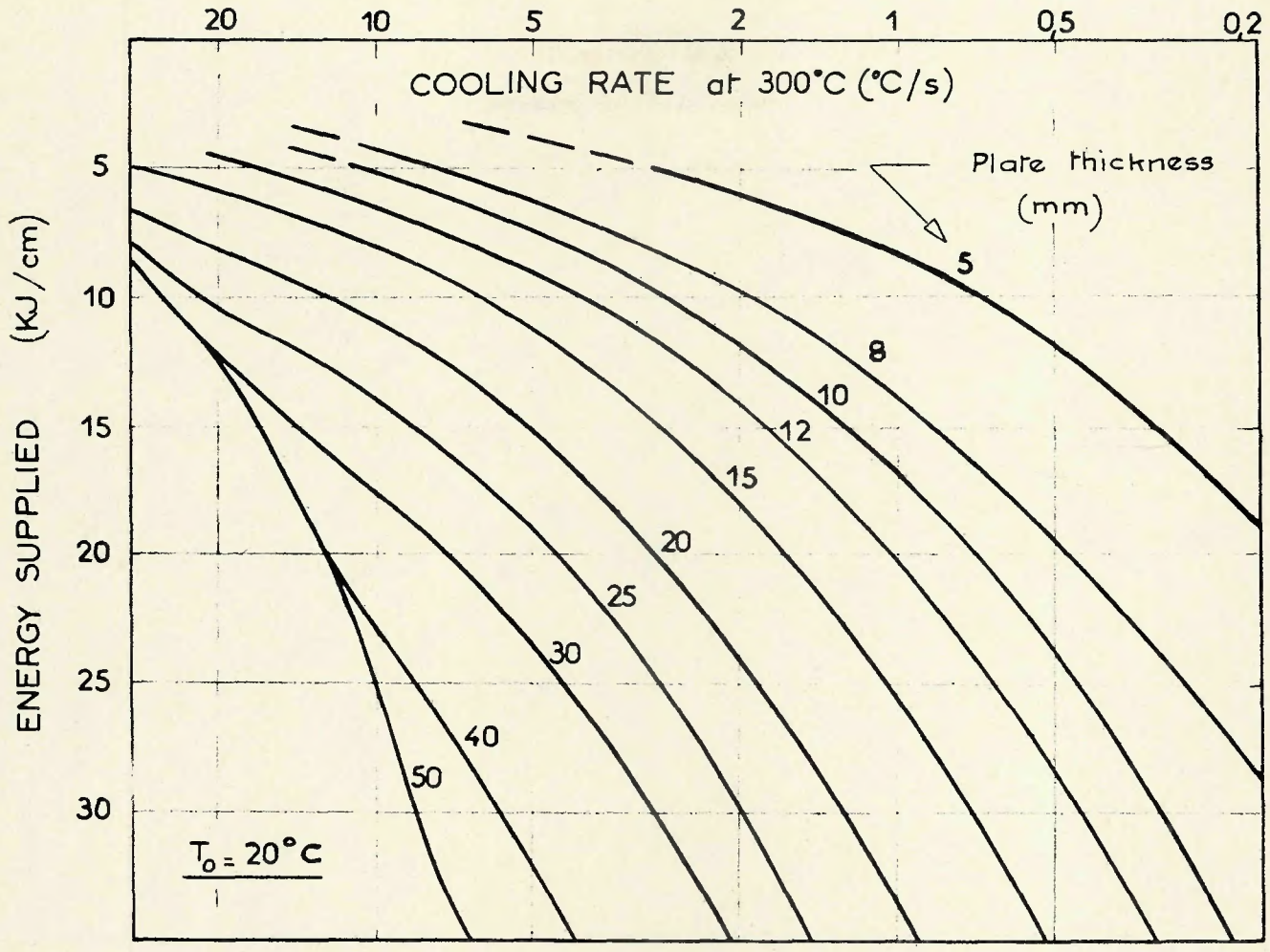


Fig. 4—Relationship between cooling rate, plate thickness and energy supplied (no preheat)

high yield weldable steels. This was thought to be essential for the weldability relations under consideration.

To clarify this paper, results are presented in detail on a single grade, an A52 steel (18M5). The results obtained on the other four grades will be described at the end of this section.

The different CTS tests carried out on the 18M5 grade are given in Fig. 6.

These different tests are identified by their corresponding TSN values. The relation between TSN and cooling rate at 300C was obtained using the energy effectively supplied to the weld. The cooling rates corresponding to each TSN value are indicated together with their individual scatter bands, since, for a given weld bead there are up to three possible sections, these being related to the energy values and hence to the cooling rates. For each of these tests, the corresponding maximum underbead hardness values are given (Vickers hardness under 5 kg load). In this way a correlation between the CTS maximum hardness and the cooling rate at 300C has been obtained.

It is seen that from 20°C/S to 3°C/S, the hardness falls from 405 to 375, whereas between 3°C/S and 1.8°C/S a more rapid drop from 375 to 310 is observed.

It will be seen later that this is explained by a martensitic structure in the former case and a mixed martensite-bainite structure in the latter.

The same procedure can be adopted for simulation tests carried out on the RPI "Gleeble" machine (shown in Fig. 7).

The material for the RPI test specimens was taken from the plate center but as close as possible (~1cm) to the weld bead from the CTS tests. The thermal cycles imposed on the test specimens were determined from Adam's nomogram. These were of the following form:

- Heating rate V = 50°C/S (unimportant)
- Austenitizing treatment equivalent to 1400C – 1 sec. The austenitizing treatment was not varied with the welding conditions, since the latter have but little influence in the range Q = 15,000 to 25,000 J/cm. Furthermore, the exact austenitizing parameter necessary for a rigorous simulation of the most severe weld "peak" was not known.
- Rates of cooling at 300C calculated from Adams's formulas, with Q selected arbitrarily in the 15,000 to 25,000 J/cm range. A number of cooling curves were drawn in this

**Table 1—Grades of Steels Studied**

| Grades | Composition, wt percent | | | | | | | | |
|---|---|---|---|---|---|---|---|---|---|
| | C | Si | S | Mn | Ni | Cr | Mo | Al total | V |
| 15M5 | 0.15 | 0.30 | 0.015 | 1.40 | 0.11 | 0.09 | 0.03 | 0.027 | |
| 18M5 | 0.175 | 0.37 | 0.016 | 1.36 | 0.22 | 0.11 | 0.04 | 0.022 | |
| 20MV4 | 0.22 | 0.34 | 0.014 | 1.14 | 0.36 | 0.18 | 0.05 | 0.026 | 0.075 |
| 16MNCD4 | 0.165 | 0.33 | 0.014 | 1.24 | 0.61 | 0.58 | 0.25 | 0.032 | |
| 18MNCD5 | 0.18 | 0.32 | 0.011 | 1.30 | 0.78 | 0.81 | 0.22 | 0.026 | |

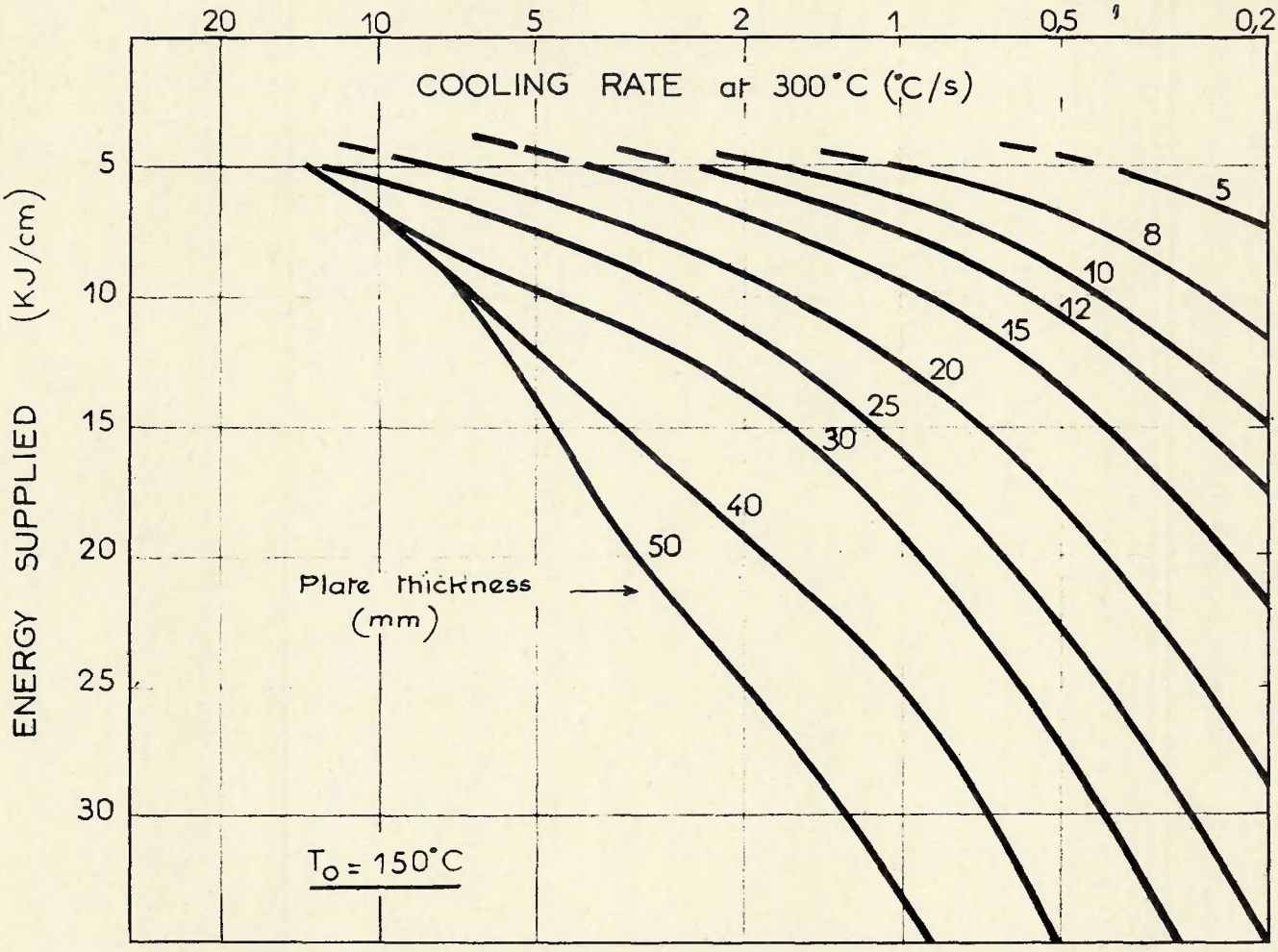


Fig. 5—Relationship between cooling rate, plate thickness and energy supplied (preheated at 150C)

way. The curves obtained correspond to cooling rates at 300C of 1, 1.5, 2.25, 3 and 6°C/S.

From the thermal cycles programmed in this way, dilatometric data (transformation start and finish temperatures) and hardness values corresponding to the resultant structures were derived (Fig. 8).

The RPI results show that the sharp temperature rise at the start of transformation (460 to 520C) is always related to an abrupt drop in hardness from 375 to 300. This corresponds to a decrease in the quantity of martensite. This method offers an accurate evaluation of the critical cooling rate for martensite formation, since the hardness and dilatometric measurements are in full agreement. The value has been determined as 2.5°C/sec.

We shall now attempt to calculate the variation in hardness for this steel. To do this we shall use various mathematical formulas obtained from continuous cooling transformation diagrams.

Consider the continuous cooling transformation diagram for a given steel, such as that for the grade 30NCII (Fig. 9). In particular, the three classical structures : martensite, bainite and ferrite-pearlite can be distingusihed together with critical rates such as $V_1$ for martensite formation, $V_2$ for bainite formation and $V_3$ for annealing. We have adopted the terminology used in a previous paper.[2]

It is preferable to report this diagram in terms of the logarithm of the cooling rate (Fig. 10). The different structures together with their relative quantities and corresponding hardness values are then more clearly apparent.

For the problem with which we are at present concerned, five experimental values are of more particular interest : the three critical rates $V_1$, $V_{1(50)}$ (50% bainite—50% martensite) and $V_2$, and the two hardnesses (martensite and bainite).

Consideration of the totality of the published continuous cooling transformation diagrams known to the authors has enabled mathematical formulas to be derived relating the above five experimental values.

The list of available diagrams which can be used for this purpose is given in Table 2. This list comprises 25 diagrams from IRSID, 44 diagrams from Max Planck Institute, 26 diagrams from CNRM, 42 diagrams from Creusot—Loire, 12 diagrams from Inagaki (Japan) and 6 diagrams from BWRA. This is a total of 155 diagrams for low alloy steels, that is steels containing less than 5% alloying elements.

However, these diagrams cannot directly be superimposed since they relate to different austenitising conditions, with temperatures ranging from 800 to 1400C, for times between 1 sec and 9 hours. To overcome this difficulty, use has been made of the equivalence parameter relating time (t) and temperature (T) described in a previous publication[3].

Thus, the logarithm of the time and the reciprocal of the absolute temperature are related via an activation energy of unique and constant value, in the present case 110 K cal/mole. The complete formulation of this equivalency, whose utility is not limited to the present application[4, 5, 6, 7], is given by the equation:

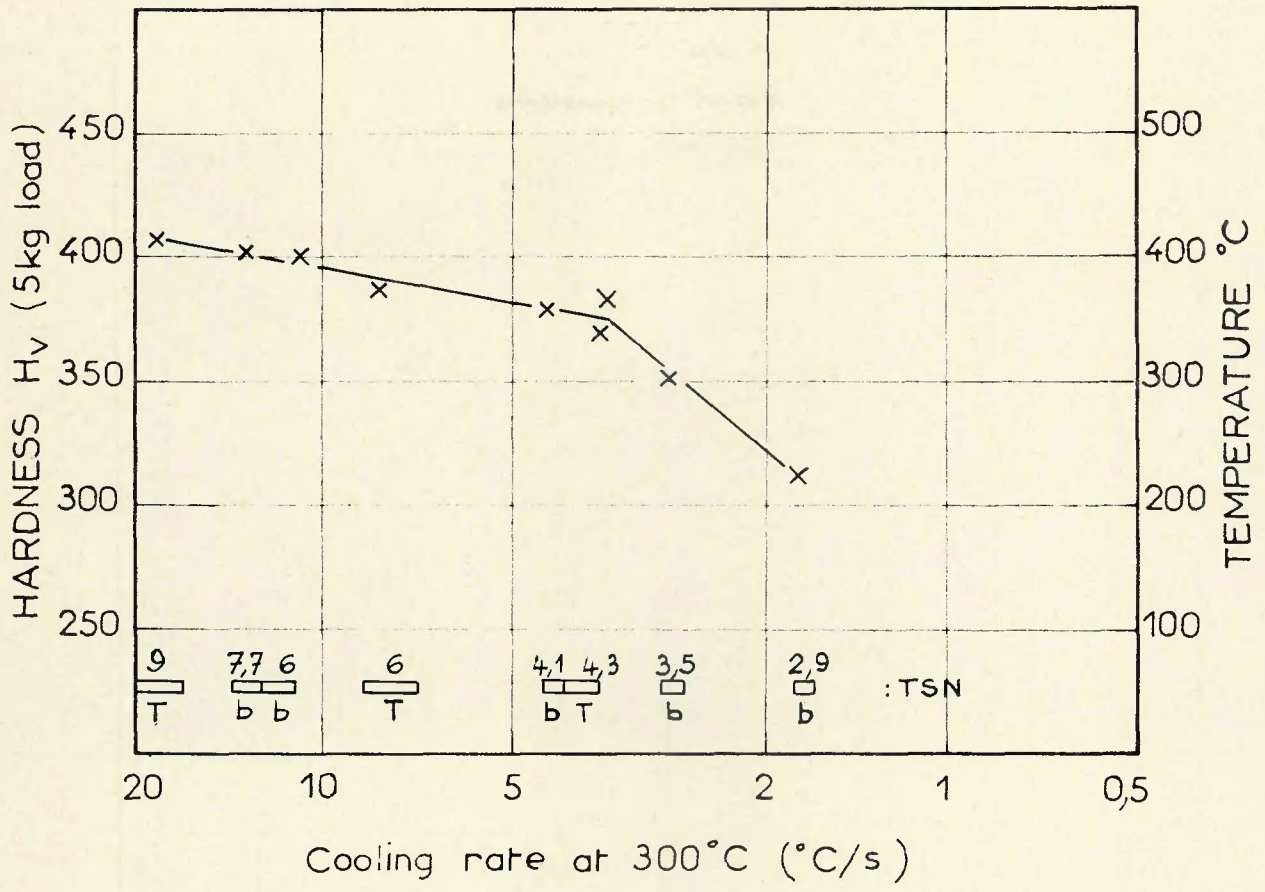


| Composition % | C | Si | S | Mn | Ni | Cr | Mo | Al | | $H_2$ ppm |
|---|---|---|---|---|---|---|---|---|---|---|
| Base metal | 0,175 | 0,37 | 0,016 | 1,36 | 0,22 | 0,11 | 0,04 | 0,022 | | |
| Electrode SCP 60 | 0,05 | | | 1,5 | | 1,17 | 0,15 | | | 5,2 |

Fig. 6—Results of CTS tests carried out on 18M5 steel

$$P = \left(\frac{I}{T} - \frac{nR}{\Delta H}\log\frac{t}{t_0}\right)^{-1}$$

where T = temperature (°K)

t = time

$t_0$ = reference time

$\Delta H$ = activation enthalpy

n = natural log of 10

R = gas constant.

A nomogram can be established to facilitate the use of this relation and each diagram can then be characterized by an austenitising parameter.

It is not necessary here to go into details of the least squares calculations carried out to determine the relations between critical rates and hardness values. Suffice it to say that formulas have been obtained which have been adapted to welding problems. For example, in the case of the three critical cooling rates of interest, three formulas are obtained and the standard error is ± 0.25;

$$\log V_1 = 3 - (4.62C + 1.05Mn + 0.54Ni + 0.50Cr + 0.66Mo)$$

$$\log V_{1(50)} = 2.4 - (4.13C + 0.8Mn + 0.57Ni + 0.41Cr + 0.94Mo)$$

$$\log V_2 = 1.9 - (3.8C + 1.07Mn + 0.7Ni + 0.57Cr + 1.58Mo)$$

The compositions are expressed in lot percent. The cooling rates are expressed in °C/sec at 300C and the austenitizing parameter, not stated specificly here, is equivalent to 1400C − 1 sec.

The above formulas are valid for all low alloy steels. It is seen that the elements Si, S, P, Al, Cu and Sn do not exert a significant influence and this is also the case for Nb and V. It should be

**Table 2—Continuous Cooling Diagrams Employed**

| Origin | Number of Diagrams C.C.T. | Classical Austenitising Temperature | Classical Austenitising Hold-Time | Weld Austenitizing Temperature | Weld Austenitizing Hold-Time |
|---|---|---|---|---|---|
| I.R.S.I.D. | 25 | $A_{c3}$ + 50 or 75C | 30 mn | 1100–1300C | None |
| Max Planck | 44 | $A_{c3}$ + 50 or 150C | 5 to 10 mn | — | — |
| C.L. | 42 | $A_{c3}$ + 30C | 1 to 9 h | 1200–1400C | 1s to 6 mn |
| C.N.R.M. | 26 | $A_{c3}$ + 50C | 30 mn | — | — |
| Inagaki (Japan) | 12 | — | — | 1350C | None |
| B.W.R.A. | 6 | — | — | 1325C | None |

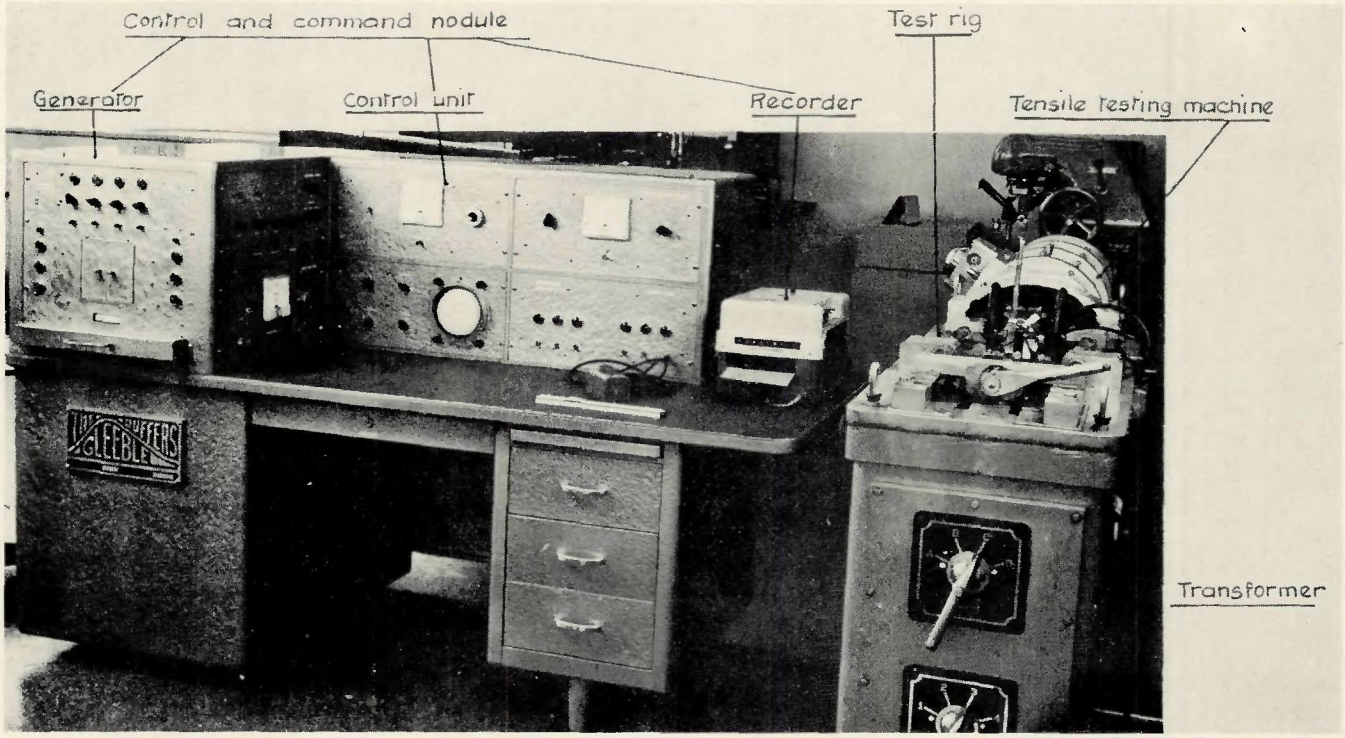


Fig. 7—Overall view of RPI Gleeble test aparatus

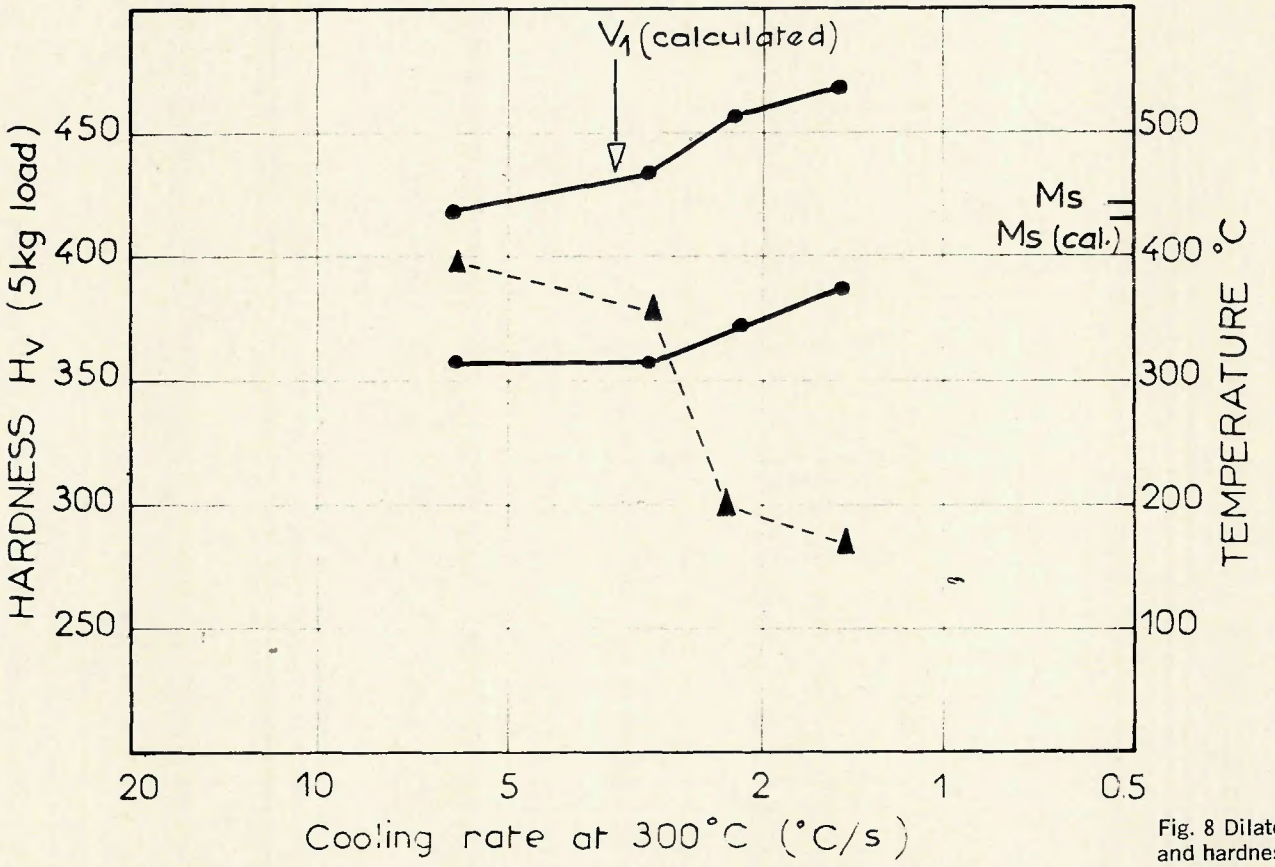


Fig. 8 Dilatometric and hardness data for 18M5 steel

| Composition % | C | Si | S | Mn | Ni | Cr | Mo | Al | | $H_2$ ppm |
|---|---|---|---|---|---|---|---|---|---|---|
| Base metal | 0,175 | 0,37 | 0,016 | 1,36 | 0,22 | 0,11 | 0,04 | 0,022 | | |
| Electrode SCP 60 | 0,05 | | | 1,5 | | 1,17 | 0,15 | | | 5,2 |

pointed out that boron steels have not been considered due to their unusual behavior, but it is known that boron does not affect the hardenability during welding cycles.

Once again nomograms have been established.

In the case of the values of Vickers hardness for martensite and bainite, two formulas have been obtained in a similar manner[8], valid with a dispersion of ± 25 HV:

$$HV\ (\text{martensite}) = 133 + 1066\,C + 29\,Si + 37.5\,Mn + 15.5\,Ni + 21.5\,Cr + 23 \log V_r$$

$$HV\ (\text{bainite}) = 72 + 337\,C + 68\,Si + 63\,Mn + 27\,Ni + 62\,Cr + 60\,Mo + 64\,V + 18 \log V_r$$

$V_r$ is expressed as usual in °C/sec and compositions in wt %. It will be noted that the coefficient for C is extremely high for martensite (1066), thereby justifying the opinion that C alone determines the hardness. For bainite on the other hand, the C coefficient is only 337.

These formulas take into account the

| C % | Mn % | Si % | S % | P % | Ni % | Cr % | Mo % | Cu % | As % | V % | W % |
|---|---|---|---|---|---|---|---|---|---|---|---|
| 0,32 | 0,30 | 0,20 | 0,008 | 0,017 | 2,95 | 0,69 | ≤ 0,10 | 0,31 | 0,056 | < 0,03 | 0,06 |

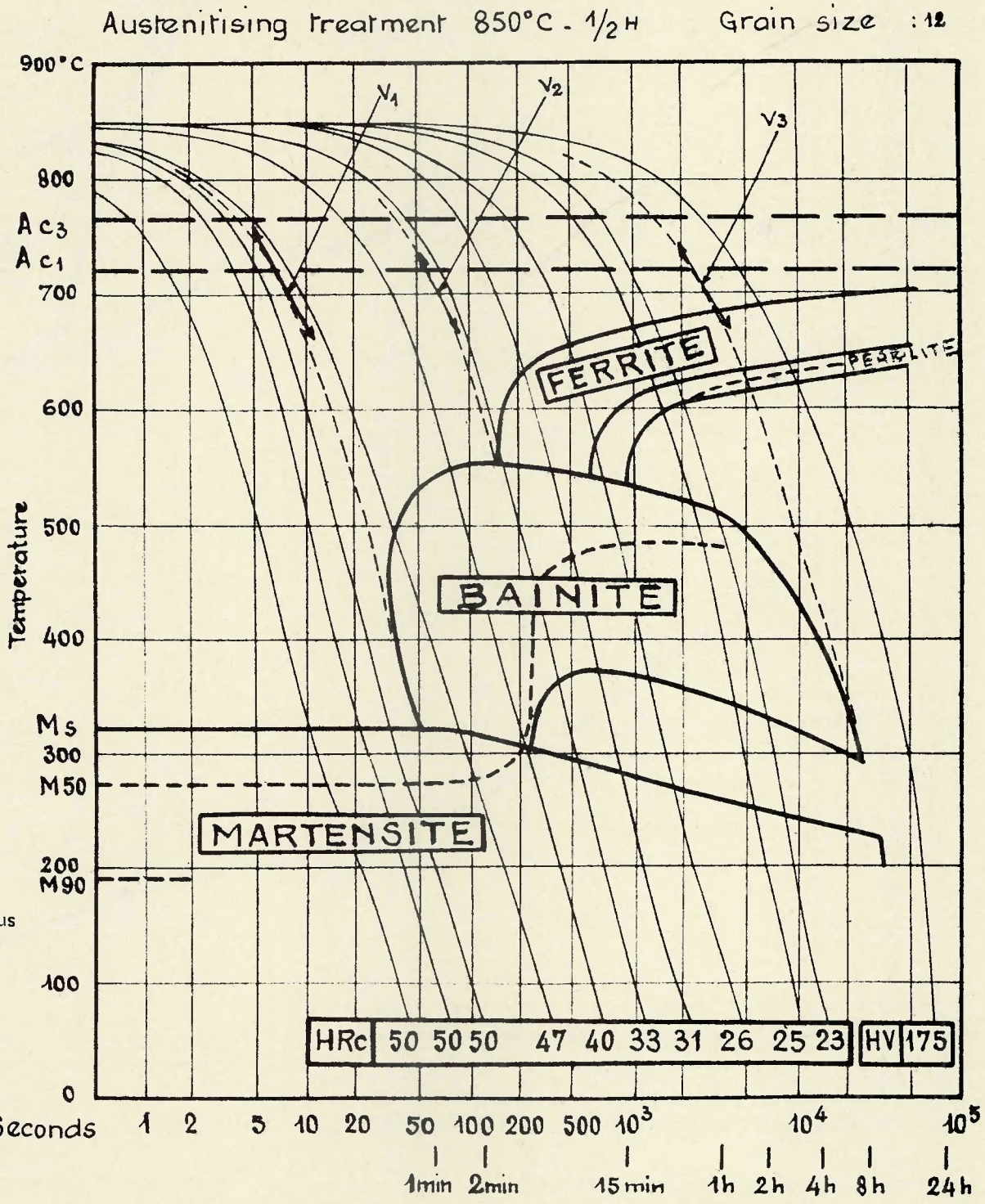


Fig. 9—Continuous cooling diagram for 30NC11 steel

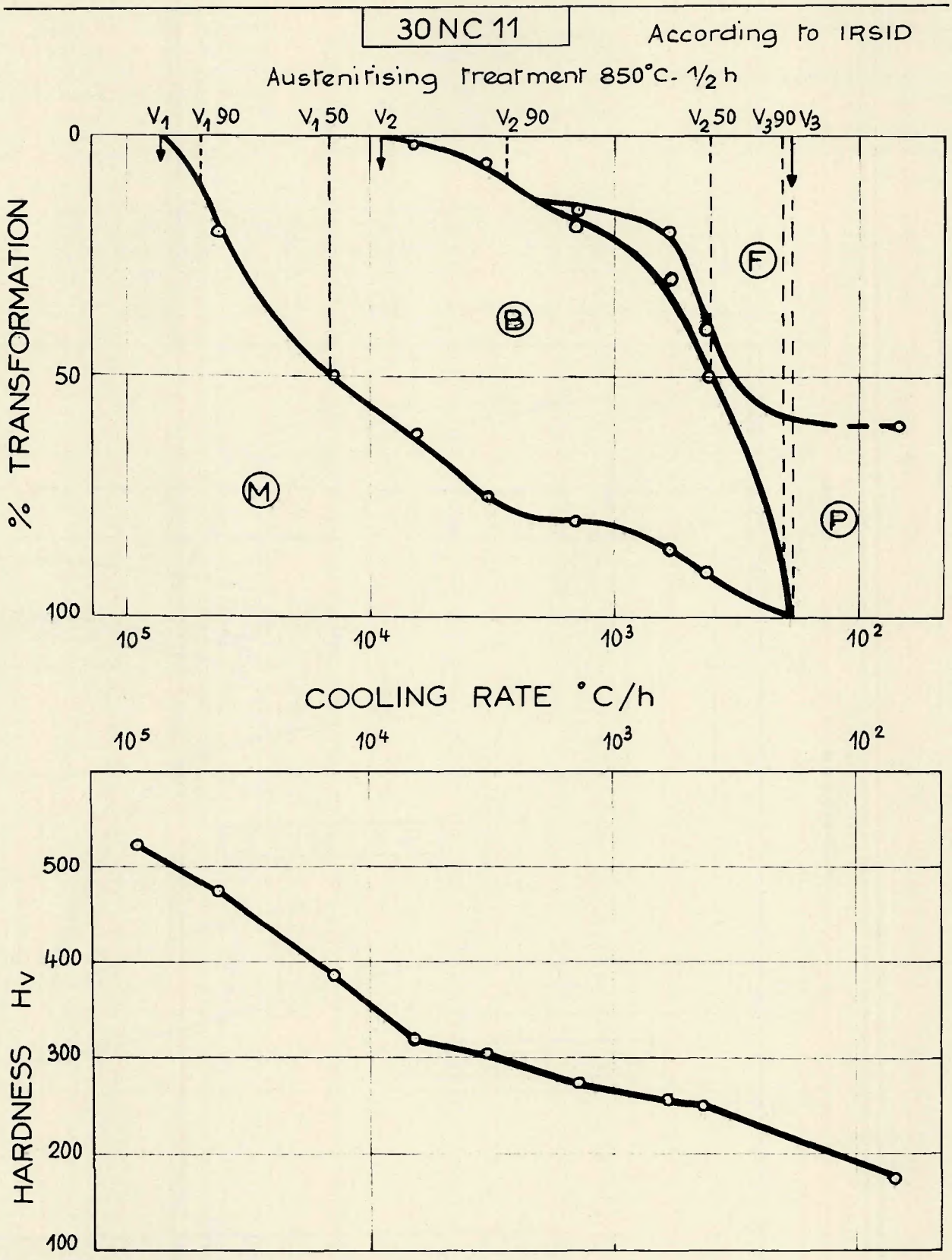


rate of cooling and therefore include auto-tempering effects. Furthermore, the elements Mo, V and Nb have no effect on martensite hardness.

Thus coming back to the steel 18M5 with these various relations, it becomes possible to calculate the hardness value corresponding to each cooling rate (Fig. 11). The first three points correspond to the hardness of the martensite and the last point to that of a mixed 50 % martensite – 50 % bainite structure.

Fig. 10—Curves in Fig. 9 have been reported to the logorithm of the cooling rate

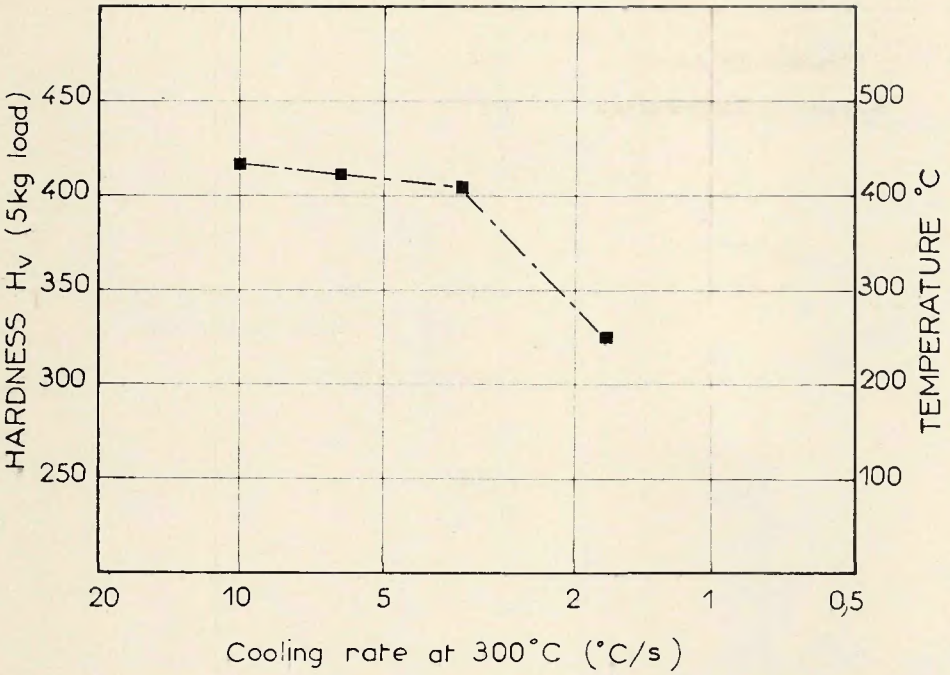


Fig. 11—Hardness value vs cooling rate for 18M5 steel

| Composition % | C | Si | S | Mn | Ni | Cr | Mo | Al | | $H_2$ ppm |
|---|---|---|---|---|---|---|---|---|---|---|
| Base metal | 0,175 | 0,37 | 0,016 | 1,36 | 0,22 | 0,11 | 0,04 | 0,022 | | |
| Electrode SCP 60 | 0,05 | | | 1,5 | | 1,17 | 0,15 | | | 5,2 |

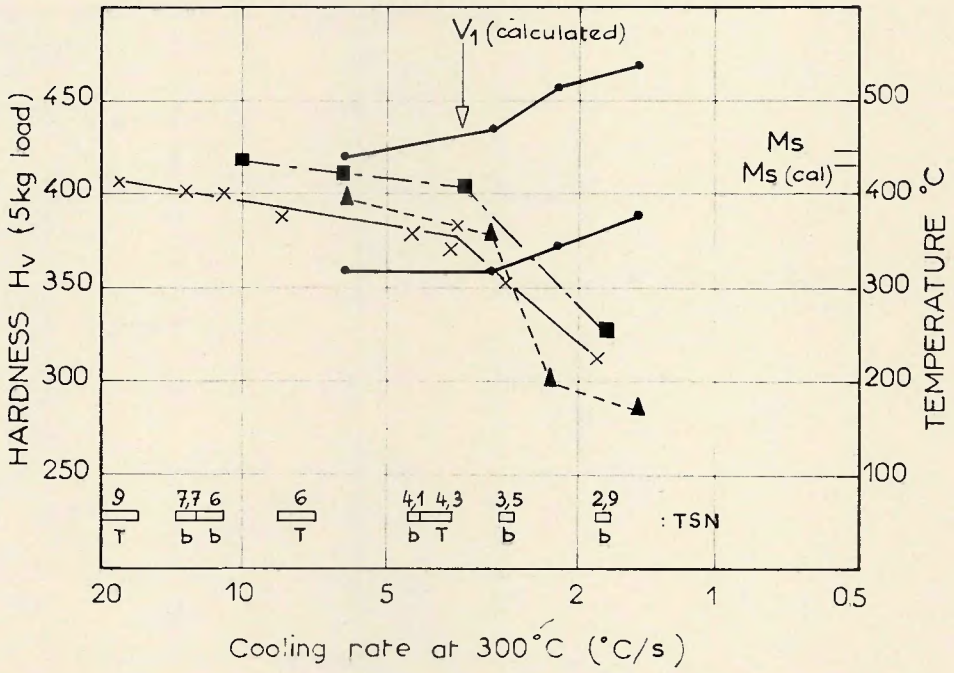


Fig. 12—All cooling rate calculations already presented have been combined here (see Figs. 6, 8 and 11)

| Composition % | C | Si | S | Mn | $N_i$ | Cr | Mo | Al | | $H_2$ ppm |
|---|---|---|---|---|---|---|---|---|---|---|
| Base metal | 0,175 | 0,37 | 0,016 | 1,36 | 0,22 | 0,11 | 0,04 | 0,022 | | |
| Electrode SCP 60 | 0,05 | | | 1,5 | | 1,17 | 0,15 | | | 5,2 |

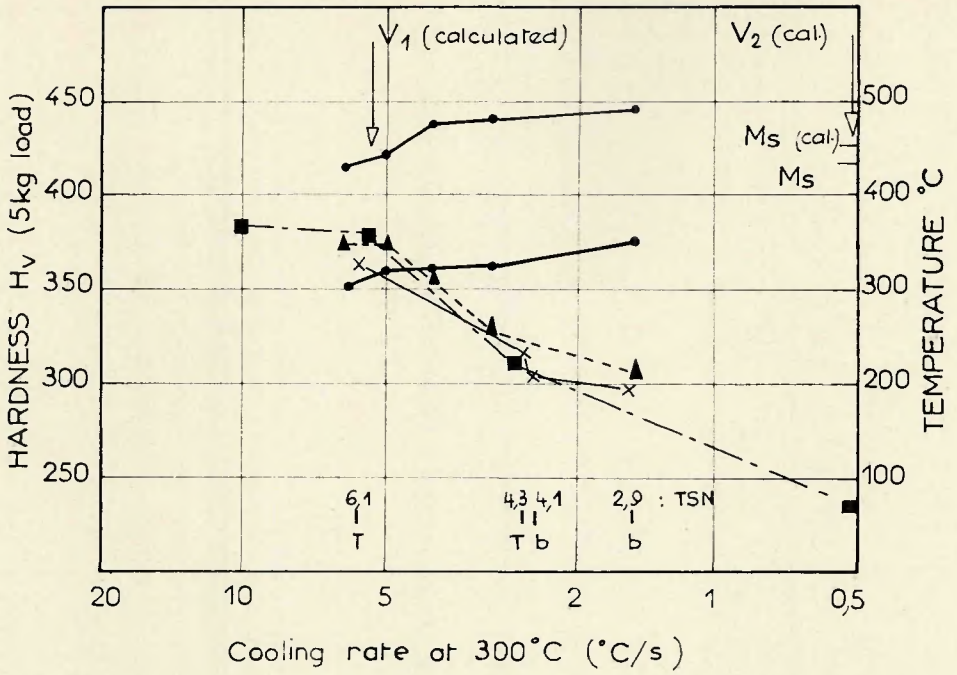


Fig. 13—Same as Fig. 12, except for steel 15M5

| Composition % | C | Si | S | Mn | N | Cr | Mo | Al | | $H_2$ ppm |
|---|---|---|---|---|---|---|---|---|---|---|
| Base metal | 0,15 | 0,30 | 0,015 | 1,40 | 0,11 | 0,09 | 0,03 | 0,027 | | |
| Electrode OK.SP 191 | 0,05 | | | 1,00 | 0,90 | | | | | 2,7 |

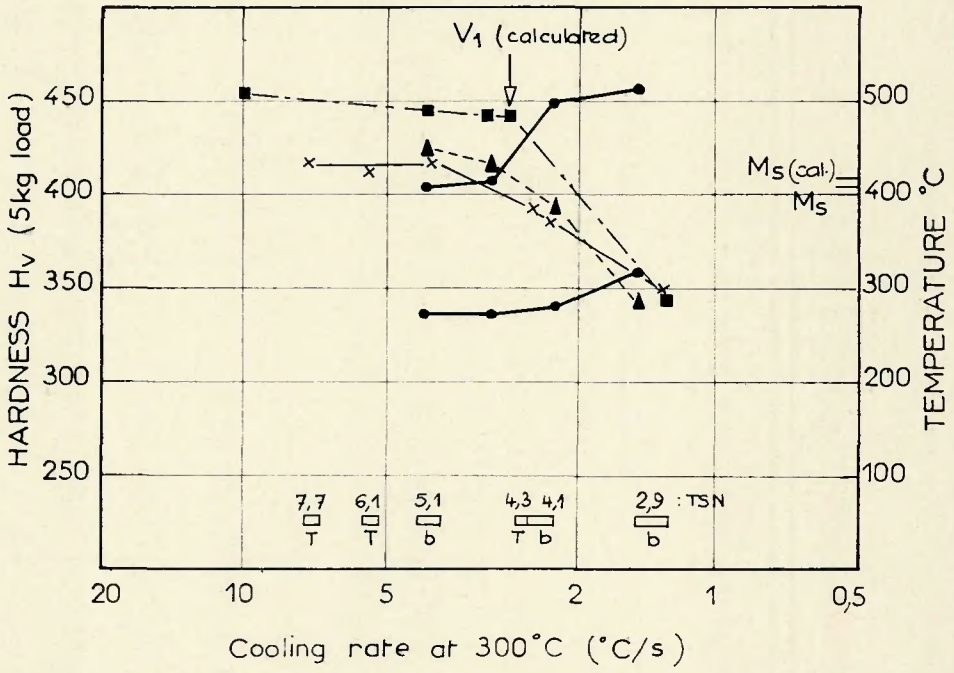


Fig. 14—Same as Fig. 12, except for steel 20MV4

| Composition % | C | Si | S | Mn | N | Cr | Mo | Al | V | $H_2$ ppm |
|---|---|---|---|---|---|---|---|---|---|---|
| Base metal | 0,22 | 0,34 | 0,014 | 1,14 | 0,36 | 0,18 | 0,05 | 0,026 | 0,075 | |
| Electrode M 45 | 0,05 | | | 0,64 | 0,055 | 0,035 | 0,05 | | | 6 |

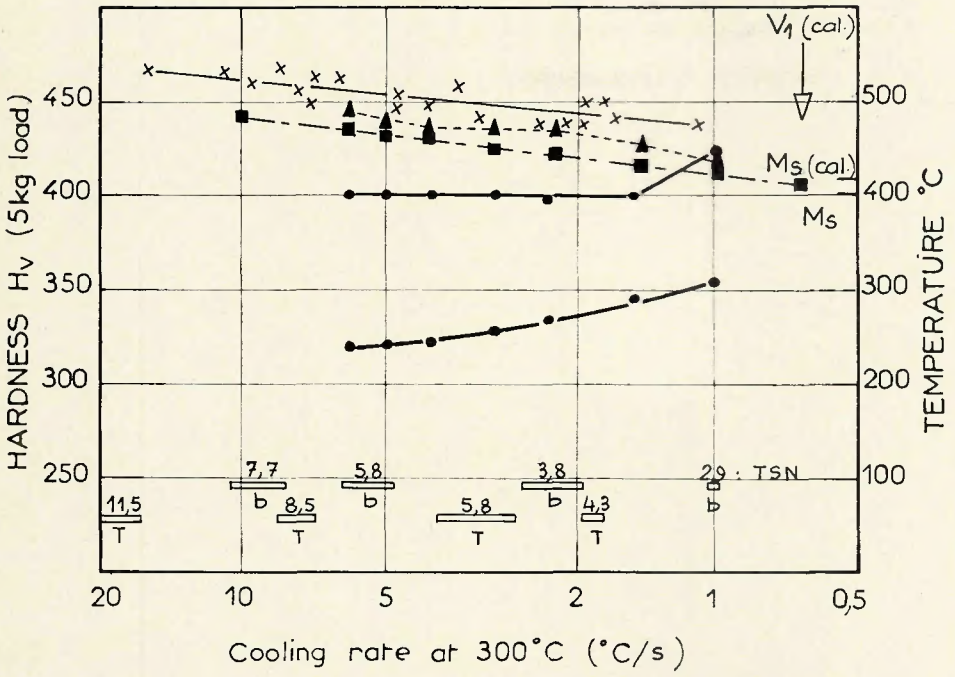


Fig. 15—Same as Fig. 12, except for steel 18MNCD5

| Composition % | C | Si | S | Mn | N. | Cr | Mo | Al | | $H_2$ ppm |
|---|---|---|---|---|---|---|---|---|---|---|
| Base metal | 0,18 | 0,32 | 0,011 | 1,30 | 0,78 | 0,81 | 0,22 | 0,026 | | |
| Electrode ND 70 | 0,07 | 0,45 | | 1,50 | 1,23 | 0,14 | 0,29 | | | 6,1<br>5,4 |

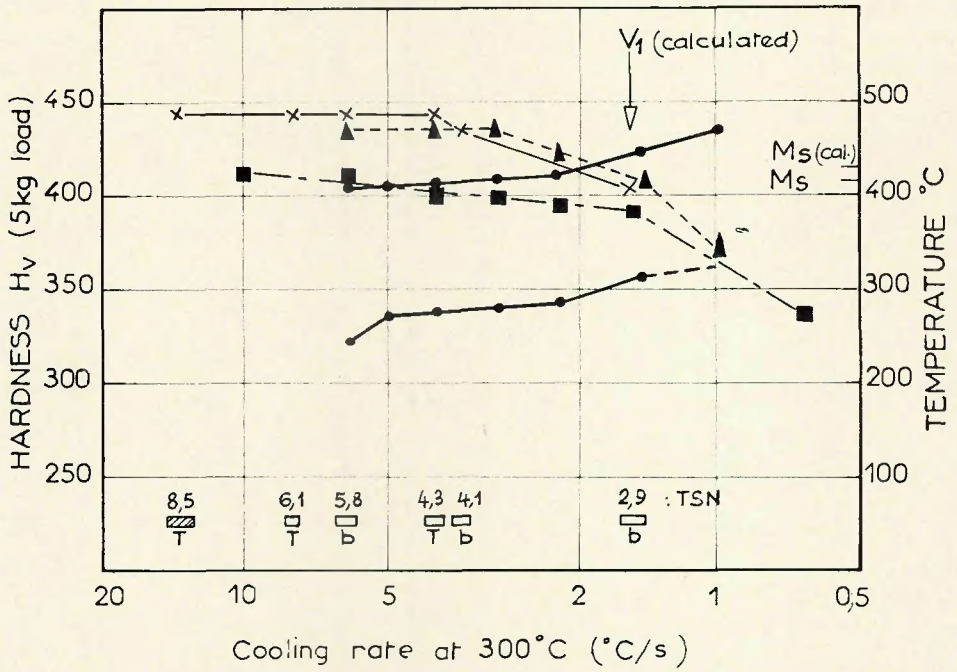


Fig. 16—Same as Fig. 12, except for steel 16MNCD4

| Composition % | C | Si | S | Mn | N; | Cr | Mo | Al | | $H_2$ ppm |
|---|---|---|---|---|---|---|---|---|---|---|
| Base metal | 0,165 | 0,33 | 0,014 | 1,24 | 0,61 | 0,58 | 0,25 | 0,032 | | |
| Electrode UL | 0,06 | | | 0,78 | 3,61 | 0,045 | 0,47 | | | 6,1 |

It now remains to superimpose the different results to see whether our various hypotheses are justified. Results for 18M5 steel are shown in Fig. 12. The dispersion does not exceed 20 HV, and the correlation is particulary satisfactory in the transition zone martensite — bainite where the scatter was expected to be greatest.

Before concluding, the results for the four other grades will be described. The steel 15M5 (Fig. 13) represents unquestionably the most convincing result, the three test series agreeing within less than 10 HV despite a mixed structure for cooling rates between 5 and 1° C/S.

For 20MV4 (Fig. 14) the calculated values are about 30 HV too high in the martensitic region.

In the case of 18MNCD5 (Fig. 15) the structure is always martensitic. The accuracy is of the order of 25 HV but it should be noted that autotempering is clearly visible and has been effectively accounted for. Finally, for the grade 16MNCD4, the calculated values are about 30 HV too low (see Fig. 16).

In general, extremely good agreement is obtained between real welding tests and RPI tests. This is not surprising since care was taken to use the same metal in both cases. On the other hand, the dispersion between experimental and calculated values is considerably greater —of the order of 25 HV. It is thought that the main reason lies in the fact that chemical compositions are not known with sufficient accuracy, particularly since 0.01 % C represents a difference in hardness of 10H V.

Nevertheless, it is felt that the original hypotheses have been confirmed and that it is possible to determine the underbead hardness by means of a knowledge of the structure.

This was the conclusion which was reached two years ago, and since then numerous additional tests have been carried out in our laboratory. It is appropriate to recapitulate the results.

## Overall Predictions—Part III

In this section two graphs are presented: one concerns the calculation of hardness measurements in RPI tests, the other in welded joints.

### Graph I

The results of 60 simulation tests performed on the RPI Gleeble machine are shown in Fig. 17, differentiated according to whether the structure was martensitic or mixed martensitic-bainitic.

It is seen that the two populations are equally centered. The mean difference between calculated and measured values for the 60 results is 1.5 HV, i.e. extremely small. The dispersion is ± 15 HV which, given the overall variation

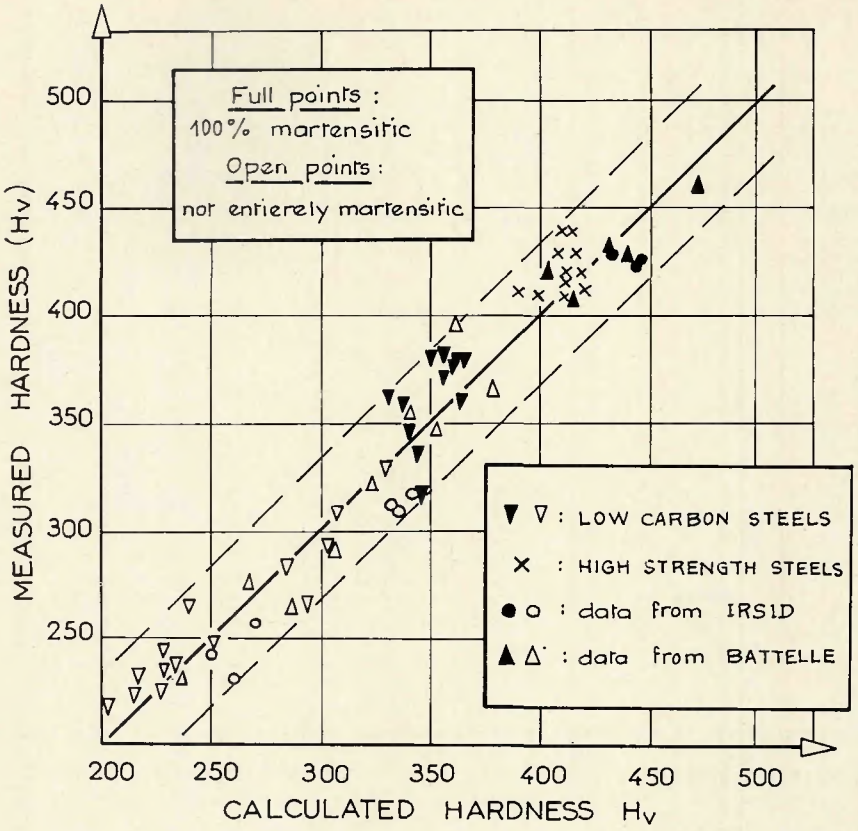


Fig. 17—Results of 60 simulation tests performed on RPI Gleeble machine

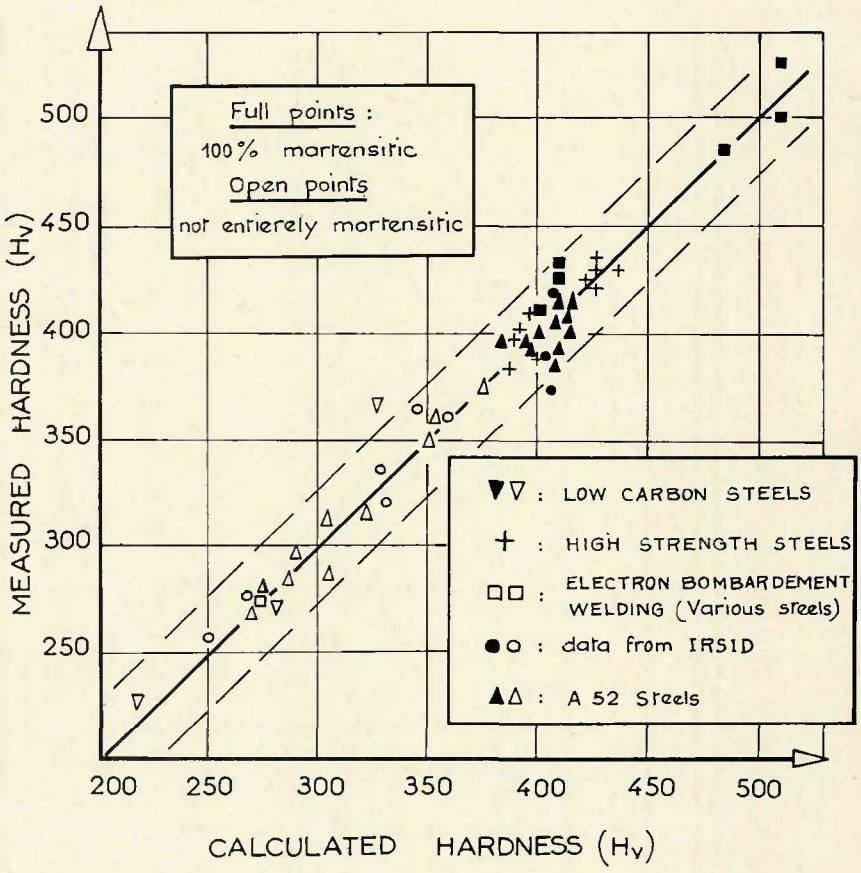


Fig. 18—Hardness measurements on 50 real weld joints are plotted

in hardness of 200 to 475 HV, can be considered satisfactory.

Note that low carbon steels (C <0.10) have been included. Although this represents an extrapolation of our formulas, the dispersion is not affected. Similarly included are the results of tests carried out under contract with Battelle Institute in Geneva on steels of a quite different type. The dispersion is once again satisfactory.

### Graph II

Measurements on 50 real weld joints are analysed in Fig. 18. It is seen that the mean difference between measured and calculated hardness values is only 0.9 HV and that the dispersion is only ± 12.5 HV for a hardness range of 200 to 525 HV. Two extrapolations merit attention, one concerning the low carbon steels already mentioned and the other relating to the welding technique, since five electron bombardment welding tests are included.

## Conclusions

It has been shown that there is an excellent correlation between underbead hardness derived from CTS or RPI Gleeble tests and that calculated from mathematical formulas valid for all low alloy steels.

Four conditions are necessary for this conclusion to be valid: (1) Calculation of cooling rates in a weld from Adams's equations, (2) a Gleeble machine, or any other heat treatment apparatus capable of programming welding cycles for both two and three dimensional heat flow, (3) use of an equivalence parameter between time and temperature enabling interrelation of continuous cooling transformation diagrams obtained for classical heat treatments (austenitising at $AC_3$ + 30C for 1 hr) and for weldability studies (peak at 1300 to 1400C), and (4) mathematical formulations relating critical quenching rates with the hardness of martensite and/or bainite as a function of steel composition. This was only possible after interpretation of more than 340 continuous cooling diagrams.

It has thus been shown that since the underbead hardness can be derived from simple metallurgical considerations, it cannot be an independent variable for a weldable steel; its value is automatically determined when the welding conditions have been fixed.

The present work puts in perspective the so-called 'equivalent carbon' formulas. Since these do not take into account plate thickness or welding conditions, they can only give approximate results.

Finally, to satisfy user requirements, easy-to-use nomograms have been established whenever possible. These are in daily use in the author's company.

However, these nomograms will soon be out of date, since it should be possible to solve the whole problem by means of computer programming. This will be the next phase of our work.

### *References*


1. Brisson, J., Maynier, Ph., Dollet, J., Bastien, P. "Underbead Hardness Study of Carbon and Low Alloy Steels," *Soudages et Techniques Connexes*, 22-11/12-Nov.-Dec., 1968.
2. Maynier, Ph., Dollet, J., Bastien, P., "Effect of Alloying Elements on the Quench Susceptibility of Low Alloy Steels," *Revue de la Métallurgie*, April, 1970.
3. Maynier, Ph., Martin, P. F., Bastien, P., Sebille, J., "The Austenitization Time-Temperature Equivalence. Its Application to Heat Treating and Welding," *Mémoires Scientifiques de la Revue de Métallurgie*, Vol. 63, Dec., 1966.
4. Maynier, Ph., Martin, P. F., Bastien, P., "An Application of the Austenitization Time-Temperature Equivalence to the Study of Hardening and Decarburizing," *Mémoires Scientifiques de la Revue de Métallurgie*, Vol 64, March, 1967.
5. Nectoux, G., Maynier, Ph., Bastien, P., "An Application of the Decarburization Study of Low Alloy Steels," *Revue de la Métallurgie*, April, 1969.
6. Pont, G., Maynier, Ph., Martin, P.F., "An Application of the Time-Temperature Equivalence to the Study of Steel Tempering," *Revue de la Métallurgie*, Vol. 64, Dec., 1967.
7. Pont, G., Maynier, Ph., Dollet, J., Bastien, P., "A Contribution to the Study of the Influence of Molybdenum upon the Activation Energy of Softening During Tempering," *Mémoires Scientifiques de la Revue de Métallurgie*, Vol. 67, Oct., 1970.
8. Maynier, Ph., "Hardness of Martenite, of Bainite and of Mixed Ferrite-Pearlite Structures," Unpublished results.
9. Adams, Jr., C. M., *Welding Journal*, Vol. 20, No. 5, p. 210-s, 1958.